Modular Redundant Manipulator Design for Dynamic Performance

Alan Bowling and Oussama Khatib
Robotics Laboratory
Department of Computer Science, Stanford University
Stanford, CA 94305, USA

Abstract

This article presents a methodology for the modular design of redundant manipulators for improved dynamic performance. The modularity is obtained from a special decomposition of the design problem into smaller more manageable subproblems. This decomposition corresponds to a division of the redundant mechanism into non-redundant macro and mini substructures that will be designed separately. The design of these substructures is based on recently developed characterizations of end-effector inertial and acceleration properties. These characterization treat the properties related to linear and angular motion separately in order to address the inhomogeneities, or differences in units, between them. The result of this analysis is a highly efficient design process. An important aspect of this analysis are the bounds it provides on the characteristics of the overall mechanism. The methodology is illustrated on the design of a six degree-of-freedom planar manipulator.

1 Introduction

In this paper, we present a modular approach to addressing the design problem for redundant robotic manipulators. This work has its foundations in our previous studies of macro/mini manipulator systems [16]. The main result from those studies employed here is that a redundant manipulator can be divided into two or more substructures whose interactions can be analyzed in order to obtain insights into the overall mechanism's behavior. These insights facilitate the decomposition of the redundant manipulator design problem into a set of smaller subproblems which consist of the separate design of the substructures.

This modular approach differs from a number of other studies that addressed redundancy by examining the mechanism in total. These earlier studies analyzed kinematics, [1, 3, 17], as well as dynamics, [14]. The global approach to design followed in these studies ensures that the resulting design has the desired performance characteristics. In our approach, this is accomplished through the analysis of substructure interactions, which results in guidelines for the substructure designs. Adherence to these guidelines allows the prediction of bounds on the overall performance characteristics.

An important implication of this decomposition is that many of the characterizations developed for non-redundant manipulators can be applied to redundant mechanism design. These characterizations for non-redundant mechanisms can be based on kinematics, [2, 10, 18, 19, 21], as well as dynamics, [4, 11, 15, 9, 20]. These studies are discussed in more detail in [8].

This article addresses the characteristics related to dynamic performance. This aspect of performance is concerned with the responsiveness of a mechanism to controller commands. Our characterizations of dynamic performance apply to the end-effector inertial and acceleration properties. They differ from the studies discussed above in that the properties related to linear and angular motion are considered separately, and do not involve any scaling factors [6, 13].
When dealing with redundant mechanisms, the effect of redundancy on the overall performance should also be considered. The proposed decomposition facilitates this analysis of *null space performance*. In the following sections the modular approach to addressing redundancy is first presented. The characterizations of dynamic performance used here are then discussed. Analysis of the substructure interactions and the predictions of overall mechanism performance characteristics are then presented. These insights and predictions are verified in a six-DOF planar redundant manipulator design example.

2 Treatment of Redundancy

A major difficulty in the analysis of redundant mechanisms involves the characterization of null space motions; joint motions which do not produce end-effector motion. The extra motion freedom provided by the null space necessitates consideration of both end-effector and null space properties. These two aspects of the design problem can be interpreted in terms of the manipulator's *task execution* and *self motion* capabilities. In this work macro/mini design concepts are used to address these two capabilities.
In macro/mini design it is assumed that the mini manipulator will govern task execution while both mechanisms will affect self motion. However, the macro manipulator is assumed to impose most of the limitations on self motion. Therefore the mini manipulator is designed independently of the macro to fulfill the task requirements. The macro manipulator is then designed to complement the performance of mini by providing self motion capabilities and also increasing the size of the workspace. Since the macro and mini manipulators are intended to fulfill different purposes, it is natural to consider decomposing the design problem into subproblems consisting of the separate design of these two mechanisms. In this decomposition the mini manipulator is defined as the distal set of links which span the motion space of the end-effector, and the macro manipulator is comprised of the remaining links. Here both mechanisms are assumed to be non-redundant.
Two constraints are placed on the design to insure fulfillment of the macro/mini design goals:

1. The macro must be able to stabilize its end-effector against all mini motion
2. The mini must be able to stabilize its end-effector against all macro motion.

The first constraint means that the macro must be capable of holding its end-effector still while the mini manipulator performs all possible motions. This constraint guarantees that the mini manipulator can execute the task while the macro acts as its fixed base. Analysis of this constraint yields a lower bound on the macro performance.
The second constraint means that the mini must be capable of holding its end-effector fixed in the workspace while the macro performs all possible motions. This constraint directly affects self motion capability, or null space performance. Since the substructures are non-redundant,

null space motion can only be produced through their interactions; the submechanisms must cancel each other's motion. Analysis of this constraint produces an upper bound on macro performance. This bound defines when the macro manipulator is overdesigned since it will have more performance than the mini can counteract in order to produce self motion.

Since the macro and mini manipulators are separately designed, the interactions between them must be analyzed in order to insure that the assembled mechanism has the desired characteristics. Therefore the constraint forces between them must appear consistently in their dynamic models. This is accomplished using a slightly modified Newton-Euler free-body diagram analysis. The free-body diagram for the macro/mini manipulator is shown in Figure 1 where the constraint forces are represented as reaction forces, labeled $\mathbf{F}_r$.

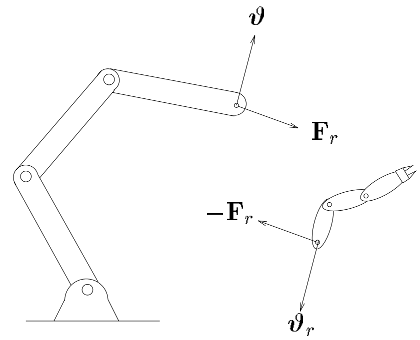

Figure 1: Macro/Mini Decomposition.

The mini manipulator's dynamic model is developed in terms of its base motion and its motion relative to the base. The base motion is described by $\boldsymbol{\vartheta}_r$, the vector of Cartesian velocities required to bring the reaction forces $\mathbf{F}_r$ into evidence in the dynamic model [12]. The velocity dependent terms will be omitted from the dynamic model because they complicate the proposed analysis considerably; only motions from rest are considered. Assuming that all quantities are expressed in the same inertial frame, the system of equations representing the dynamic model for the macro/mini manipulator can be expressed as

$$A_{\mathrm{M}}\, \ddot{\mathbf{q}}_{\mathrm{M}} \;+\; \mathbf{g}_{\mathrm{M}} \;+\; J_{\mathrm{M}}^T\, \mathbf{F}_r \;=\; \mathsf{G}_{\mathrm{M}}\, \boldsymbol{\Upsilon}_{\mathrm{M}} \;=\; \boldsymbol{\Gamma}_{\mathrm{M}} \tag{1}$$

$$\begin{bmatrix} \Lambda_{\mathrm{m}_r} & A_{\mathrm{m}_c} \\ A_{\mathrm{m}_c}^T & A_{\mathrm{m}} \end{bmatrix} \begin{bmatrix} \dot{\boldsymbol{\vartheta}}_r \\ \ddot{\mathbf{q}}_{\mathrm{m}} \end{bmatrix} + \begin{bmatrix} \mathbf{g}_{\mathrm{m}_r} \\ \mathbf{g}_{\mathrm{m}} \end{bmatrix} = \begin{bmatrix} \mathbf{F}_r \\ \mathsf{G}_{\mathrm{m}} \boldsymbol{\Upsilon}_{\mathrm{m}} \end{bmatrix} \tag{2}$$

$$\dot{\boldsymbol{\vartheta}}_r \;=\; \dot{\boldsymbol{\vartheta}}_{\mathrm{M}} \tag{3}$$

In the above equations the "M" subscripted quantities refer to the macro manipulator while the "m" subscripted quantities refer to the mini manipulator. In equation (2), $\mathbf{q}_{\mathrm{m}}$ is the set of n joint coordinates describing the motion of the mini relative to its base. The subscripted quantities A, $\mathbf{g}$, $\boldsymbol{\Gamma}$, $\boldsymbol{\Upsilon}$, and G, are mass matrices, gravity forces, joint torques, actuator torques, and transformations between actuator and joint torques. Λ_{m_r} represents the inertial properties of the mini perceived at its base.

In order to explore the end-effector properties, these quantities are transformed from joint to end-effector/operational space using the Jacobian, J, defined as

$$\boldsymbol{\vartheta} \;\triangleq\; J\, \dot{\mathbf{q}} \tag{4}$$

$$\boldsymbol{\Gamma} \;=\; \mathsf{G}\boldsymbol{\Upsilon} \;=\; J^T\, \mathbf{F} \;\triangleq\; J^T \begin{bmatrix} \boldsymbol{\mathcal{F}} \\ \boldsymbol{\mathcal{M}} \end{bmatrix} \tag{5}$$

where $\boldsymbol{v}$ and $\boldsymbol{\omega}$ are vectors of end-effector linear and angular velocities, and $\boldsymbol{\mathcal{F}}$ and $\boldsymbol{\mathcal{M}}$ are the end-effector contact forces and moments.

3 Characterizations of Dynamic Performance

As stated earlier, our analysis of dynamic performance centers around characterizing end-effector inertial properties and end-effector acceleration capability. The characterizations were developed in order to provide a separate description of the properties related to linear and angular motion without the use of scaling factors.

3.1 Inertial Properties

The inertial properties as perceived at the end-effector are described by the pseudo-kinetic energy matrix Λ, where $\Lambda^{-1} = J\ A^{-1}\ J^T$. Analysis of Λ is based on a decomposition of the Jacobian matrix into its linear and angular sub-matrices:

$$J = \begin{bmatrix} J_v \\ J_\omega \end{bmatrix} \tag{6}$$

where the matrix J_v transforms joint velocities into end-effector linear velocities and J_ω does likewise for end-effector angular velocities. From these relationships the mass and inertia properties are described by the matrices, Λ_v and Λ_ω;

$$\Lambda_v = (J_v\ A^{-1}\ J_v^T)^{-1} \qquad \text{and} \qquad \Lambda_\omega = (J_\omega\ A^{-1} J_\omega^T)^{-1}. \tag{7}$$

3.2 Acceleration Characteristics

In this section a brief discussion of the characterization for end-effector and null space acceleration capability is presented. More details are available in [5, 6, 8]. Here end-effector acceleration capability is explored by determining the isotropic acceleration, the largest magnitude of acceleration possible in or about every direction. The dynamic model, equation (1) for example, the symmetric bounds on actuator torques,

$$-\boldsymbol{\Upsilon}_{bound} \ \leq\ \boldsymbol{\Upsilon}\ \leq\ \boldsymbol{\Upsilon}_{bound}, \tag{8}$$

and the Jacobian are used to develop the model for this analysis,

$$\boldsymbol{\Upsilon}_{lower}\ \leq\ E_v \dot{\boldsymbol{v}}\ +\ E_\omega \dot{\boldsymbol{\omega}}\ +\ \mathcal{E}_{\mathcal{F}} \boldsymbol{\mathcal{F}}\ +\ \mathcal{E}_{\mathcal{M}} \boldsymbol{\mathcal{M}}\ \leq\ \boldsymbol{\Upsilon}_{upper} \tag{9}$$

where

$$E = [\ E_v\ \ E_\omega\ ] = \mathsf{G}^{-1}\ A\ J^{-1} \tag{10}$$

$$\mathcal{E} = [\ E_{\mathcal{F}}\ \ E_{\mathcal{M}}\ ] = \mathsf{G}^{-1}\ J^T \tag{11}$$

$$\boldsymbol{\Upsilon}_{lower} = -\boldsymbol{\Upsilon}_{bound} - \mathsf{G}^{-1}\mathbf{g} \tag{12}$$

$$\boldsymbol{\Upsilon}_{upper} = \boldsymbol{\Upsilon}_{bound} - \mathsf{G}^{-1}\mathbf{g}. \tag{13}$$

Equation (9) can be expressed in terms of the magnitudes of its vector quantities, yielding what are referred to as the *isotropy equations*,

$$\mathsf{A} \begin{bmatrix} \|\dot{\boldsymbol{v}}\| \\ \|\dot{\boldsymbol{\omega}}\| \end{bmatrix} + \mathsf{F} \begin{bmatrix} \|\boldsymbol{\mathcal{F}}\| \\ \|\boldsymbol{\mathcal{M}}\| \end{bmatrix} = \boldsymbol{\Upsilon}_o \tag{14}$$

where A is developed from E in the equation (9), as is F from $\mathcal{E}$, and $\boldsymbol{\Upsilon}_{\mathrm{o}}$ from $\boldsymbol{\Upsilon}_{upper}$ and $\boldsymbol{\Upsilon}_{lower}$. The relations in equation (14) describe the isotropic magnitudes of acceleration and force which saturate at least one actuator. The acceleration and force directions which correspond to these isotropic magnitudes are also available from the analysis.

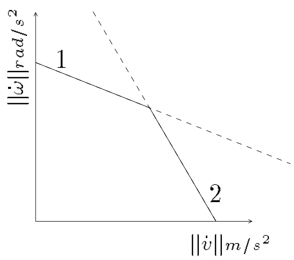

Figure 2: Motion Isotropy Curve.

Each relation in equation (14) represents a hyperplane in a four-dimensional space. The relationship between the isotropic quantities is described by the innermost envelope encompassing the origin formed when the hyperplanes are overlayed in the same space. This faceted hypersurface cannot be displayed and thus only sections of it are shown. The lines obtained from the intersection of the hyperplanes with $\|\boldsymbol{\mathcal{F}}\| = \|\boldsymbol{\mathcal{M}}\| = 0$ are shown in Figure 2. The innermost envelope is shown in solid lines and is referred to as the *motion isotropy curve*. The *force isotropy curve* can be obtained using the sectioning hyperplanes $\|\dot{\boldsymbol{v}}\| = \|\dot{\boldsymbol{\omega}}\| = 0$. The numeric labels in the figure denote the actuator which saturated providing the isotropic accelerations along that segment of the curve.

4 Analysis of Interactions

Since the mini manipulator is designed first in this process, the aim of the following analysis is to determine requirements on the macro manipulator so that it can be designed to complement the mini manipulator. As stated earlier, the velocity dependent terms in the dynamic model are difficult to address in this analysis and thus are omitted. Therefore the following analysis addresses motions initiated from rest. The following relations are developed for a manipulator with twelve degrees-of-freedom (DOF) comprised of non-redundant macro and mini manipulators. Other cases are easily derived from this one, the details of which are presented in [5].

4.1 First Constraint

The first constraint requires the macro to remain motionless, $\dot{\boldsymbol{\vartheta}}_{\mathrm{M}} = \mathbf{0}$, while the mini moves. Thus equation (2) becomes

$$A_{\mathrm{m}_c}\,\ddot{\mathbf{q}}_{\mathrm{m}} + \mathbf{g}_{\mathrm{m}_r} = \mathbf{F}_r \tag{15}$$

$$A_{\mathrm{m}}\,\ddot{\mathbf{q}}_{\mathrm{m}} + \mathbf{g}_{\mathrm{m}} = \mathsf{G}_{\mathrm{m}}\,\boldsymbol{\Upsilon}_{\mathrm{m}} \tag{16}$$

Under these conditions interactions between the mini and its base are described by the reaction forces the mini transmits to its base. The goal here is to determine the maximum magnitude of reaction force and moment the mini that the mini transmits to the macro. Eliminating $\ddot{\mathbf{q}}_{\mathrm{m}}$ from equations (15) and (16) yields

$$A_{\mathrm{m}_c}\,A_{\mathrm{m}}^{-1}\,\mathsf{G}_{\mathrm{m}}\,\boldsymbol{\Upsilon}_{\mathrm{m}} + \left(\mathbf{g}_{\mathrm{m}_r} - A_{\mathrm{m}_c}\,A_{\mathrm{m}}^{-1}\,\mathbf{g}_{\mathrm{m}}\right) = \begin{bmatrix} \mathcal{F}_r \\ \mathcal{M}_r \end{bmatrix}. \tag{17}$$

The maximum magnitude of force and moment is obtained numerically by formulating two constrained maximization problems. These problems consist of the maximization of $\mathcal{F}_r^T \mathcal{F}_r$, obtained from the first rows of equation (17), and $\mathcal{M}_r^T \mathcal{M}_r$, obtained from the last rows of equation (17), at a specified configuration subject to the constraints on the mini manipulator actuator torque capacities. The macro is designed to be capable of canceling these maximum magnitudes of force and moment in and about every direction.

4.2 Second Constraint

The second constraint can be interpreted as a direct requirement on the null space motions. The goal here is to determine the maximum isotropic acceleration of the base that the mini can counteract so that its end-effector remains motionless in the workspace. Omitting the velocity dependent terms, the kinematic requirements for null space motion are developed from the following relations,

$$\dot{\boldsymbol{v}}_e = \dot{\boldsymbol{v}}_{\mathrm{M}} + \dot{\boldsymbol{v}}_{\mathrm{m}} + \dot{\boldsymbol{\omega}}_{\mathrm{M}} \times \mathbf{p}_{\mathrm{m}} \tag{18}$$

$$\dot{\boldsymbol{\omega}}_e = \dot{\boldsymbol{\omega}}_{\mathrm{M}} + \dot{\boldsymbol{\omega}}_{\mathrm{m}}. \tag{19}$$

where the "e" subscripted quantities indicate the overall end-effector accelerations and $\mathbf{p}_{\mathrm{m}}$ is the position vector pointing from the mini manipulator base to its end-effector. The conditions under which null space motion occur, $\dot{\boldsymbol{v}}_e = \dot{\boldsymbol{\omega}}_e = \mathbf{0}$, can be expressed as

$$\begin{array}{rcl} \dot{\boldsymbol{v}}_{\mathrm{m}} & = & -\dot{\boldsymbol{v}}_{\mathrm{M}} - \dot{\boldsymbol{\omega}}_{\mathrm{M}} \times \mathbf{p}_{\mathrm{m}} \\ \dot{\boldsymbol{\omega}}_{\mathrm{m}} & = & -\dot{\boldsymbol{\omega}}_{\mathrm{M}} \end{array} \quad \Longrightarrow \quad \dot{\boldsymbol{\vartheta}}_{\mathrm{m}} = -\hat{P}_{\mathrm{m}}\, \dot{\boldsymbol{\vartheta}}_{\mathrm{M}} \tag{20}$$

where if $\mathbf{p} = [\mathrm{p}_1\ \mathrm{p}_2\ \mathrm{p}_3]^T$,

$$\hat{P} = \begin{bmatrix} \mathrm{I} & \hat{\mathbf{p}} \\ 0 & \mathrm{I} \end{bmatrix} \qquad \text{and} \qquad \hat{\mathbf{p}} = \begin{bmatrix} 0 & \mathrm{p}_3 & -\mathrm{p}_2 \\ -\mathrm{p}_3 & 0 & \mathrm{p}_1 \\ \mathrm{p}_2 & -\mathrm{p}_1 & 0 \end{bmatrix}. \tag{21}$$

Equation (20) and the Jacobian can be used to transform equation (2) as follows

$$\left(\Lambda_{\mathrm{m}_r} - A_{\mathrm{m}_c} J_{\mathrm{m}}^{-1} \hat{P}_{\mathrm{m}} \right) \dot{\boldsymbol{\vartheta}}_{\mathrm{M}} + \mathbf{g}_{\mathrm{m}_r} = \mathbf{F}_r \tag{22}$$

$$A_{dep}\, \dot{\boldsymbol{\vartheta}}_{\mathrm{M}} + \mathbf{g}_{\mathrm{m}_r} = \tag{23}$$

$$\left(A_{\mathrm{m}_c}^T - A_{\mathrm{m}} J_{\mathrm{m}}^{-1} \hat{P}_{\mathrm{m}} \right) \dot{\boldsymbol{\vartheta}}_{\mathrm{M}} + \mathbf{g}_{\mathrm{m}} = \mathsf{G}_{\mathrm{m}}\, \boldsymbol{\Upsilon}_{\mathrm{m}}. \tag{24}$$

Equation (24) describes the mini manipulator actuator effort required to counteract base motion, in order to produce null space motion. Using the bounds on the mini manipulator actuator torques, a set of isotropy equations can be developed from equation (24) which describe the isotropic accelerations of the base which can be canceled by the mini manipulator. These equations are used to develop a curve similar to that of Figure 2 which describes the bounds on mini manipulator base motion.

A macro designed to have a higher performance than suggested by this curve can be considered overdesigned although overdesigning will insure a certain level of null space performance. A macro manipulator designed with less performance is considered underdesigned and will reduce the null space performance of the overall mechanism. The development of these upper bounds is the main improvement over the early work done on this methodology [7].

However, also note that equation (22) defines a dependency base accelerations and the reaction forces required to produce those motions. Thus the macro end-effector, when attached to the mini base, will experience both an applied force and an acceleration. Since these two quantities are independent in the macro manipulator dynamic model, equation (1), the correspondence between acceleration and force must be established in order to specify design requirements on the macro end-effector which are consistent with the forces and accelerations at the mini manipulator base. This can be accomplished by substituting equation (22) into the macro manipulator dynamic model during the macro design stage. Therefore A_{dep} and $\mathbf{g}_{\mathbf{m}_r}$ must be passed to the macro design stage. The resulting dynamic model used to satisfy the second constraint in the macro manipulator design is

$$\left(A_{\mathrm{M}} + J_{\mathrm{M}}^T A_{dep} J_{\mathrm{M}} \right) \ddot{\mathbf{q}}_{\mathrm{M}} + \left(\mathbf{g}_{\mathrm{M}} + J_{\mathrm{M}}^T \mathbf{g}_{\mathbf{m}_r} \right) = \mathsf{G}_{\mathrm{M}} \boldsymbol{\Upsilon}_{\mathrm{M}}. \tag{25}$$

5 Overall Mechanism Characteristics

In order for this decomposition to be useful, bounds on the characteristics of the overall manipulator must be determinable from the substructure designs. The following predictions are valid only for a specific configuration.

1. The end-effector inertial properties of the redundant manipulator will be bounded above by the inertial properties of the structure formed by the smallest distal set of degrees-of-freedom that span the operational space, [13]

2. The end-effector isotropic accelerations at zero velocity will be bounded below by the mini manipulator end-effector isotropic acceleration capability,

3. The null space isotropic accelerations at zero velocity will be bounded above by the motion isotropy curve representing the bounds on mini manipulator base acceleration determined in Section 4.2.

The second prediction is true because the macro manipulator is designed with the capability of being a fixed base for the mini manipulator. Therefore the overall manipulator should always be capable of at least providing the mini manipulator performance. The third conclusion is true if the null space motions are considered in terms of macro end-effector motion. In this case the acceleration bound determined in Section 4.2 is truly the largest amount of acceleration which the mini can counteract.

6 Application

Here the proposed methodology is applied to the design of a six-DOF planar mechanism shown in Figure 1. The mechanism is comprised of solid cylindrical rods with actuators mounted at the joints. Only one configuration of the manipulator is examined in order to illustrate the conclusions drawn in Section 5. The relative angles between each link from the base to the end-effector are $\{ 135°, -70°, -70°, 90°, -50°, 10° \}$.

As discussed earlier, the isotropy curve in Figure 2 describes the isotropic accelerations which saturate at least one actuator, indicated by the labels adjacent to the line segments. This suggests that increasing certain actuators may improve performance. This problem has been addressed by the development of a constrained optimization problem for determining the smallest actuators which can provide a desired level of performance. The desired performance is described by specifying desired points on the hypersurface, ($\|\dot{\boldsymbol{v}}_d\|_{m/s^2}$, $\|\dot{\boldsymbol{\omega}}_d\|_{rad/s^2}$, $\|\boldsymbol{\mathcal{F}}_d\|_N$, $\|\boldsymbol{\mathcal{M}}_d\|_{Nm}$), referred to as *performance points*. The procedure chooses actuators such that these points lie on or below the hypersurface. This optimization is used in this example although it will not be discussed here in detail.

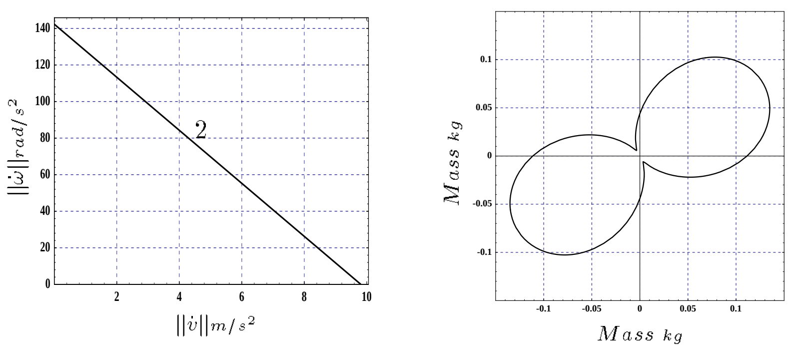

Figure 3: Mini Manipulator Properties.

The mini manipulator chosen for this example has links 10_{cm} long and 1_{cm} in diameter and is designed to provide 1_g of isotropic linear acceleration from rest, specified as $(9.81_{m/s^2}, 0, 0, 0)$. The isotropy curve and belted-inertia-ellipsoid [13], representing the end-effector mass properties for the mini manipulator design, are shown in Figure 3.

The end-effector inertia for this mechanism is 0.0000479_{kgm^2}.

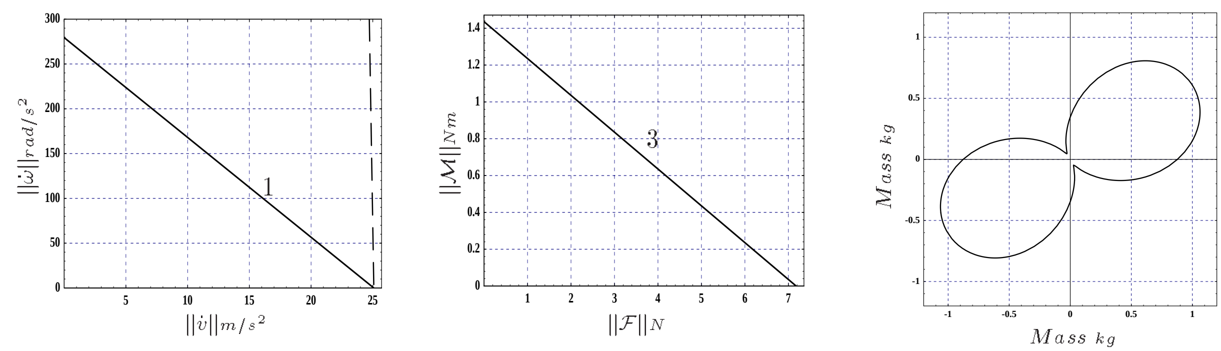

Figure 4: Macro Manipulator Properties.

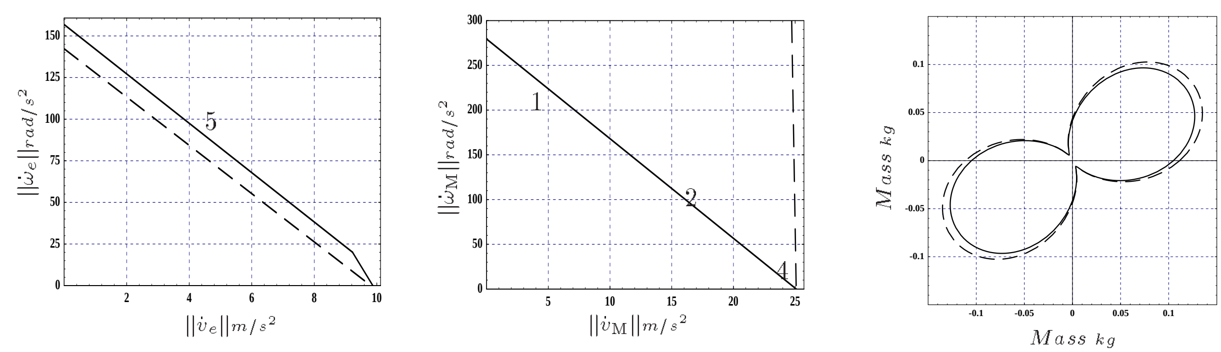

Figure 5: Macro/Mini Manipulator Properties.

The lower bound on macro performance determined from this mini manipulator design, as per

Section 4.1, is specified as two performance points: $(0, 0, 5.3_N, 0.25_{Nm})$ which corresponds to the maximum (linear) reaction force, and $(0, 0, 1.3_N, 0.252_{Nm})$, which corresponds to the maximum reaction moment. The upper bound, determined as per Section 4.2, is specified by one performance point $(25.1_{m/s^2}, 0, 0, 0)$. Only one point is chosen to represent this bound because the angular accelerations associated with other possible points are extremely large. The actuators of the macro manipulator are chosen to satisfy these three performance points.

The macro manipulator has links 20_{cm} long and 2_{cm} in diameter. The results from the macro actuator selection are shown in Figure 4. The solid line in the leftmost plot shows the motion isotropy curve for the macro manipulator and the dashed line represents the bound on macro isotropic acceleration capability determined from the mini manipulator. Note that the allowable angular acceleration can become very large. The solid line in the middle plot shows the macro manipulator force isotropy curve. Note that the first two performance points for the macro lie beneath this curve. The macro end-effector mass properties, which are much larger than the mini's, are shown in the rightmost plot of Figure 4 and its end-effector inertia is 0.0016_{kgm^2}.

The overall properties of the macro/mini manipulator are shown in Figure 5. The leftmost figure shows the end-effector accelerations with zero null space motion. The dashed line represents the mini manipulator performance shown in Figure 3. Note that the macro curve is above the mini performance as predicted in Section 5. The solid line in the middle plot describes the null space acceleration capability at zero end-effector acceleration and the dashed line shows bound on acceleration capability determined from the mini manipulator design. Here the null space motion is described in terms of the of the macro manipulator end-effector. The null space motion isotropy curve is below or equal to the bound, as predicted in Section 5.

Finally, the end-effector mass properties of the overall manipulator are shown along with the mini manipulator mass properties in the rightmost plot and are clearly smaller or equal to those of the mini, as predicted in Section 5. The overall end-effector inertia, 0.000047865_{kgm^2}, is also less than the mini's, 0.0000479_{kgm^2}.

7 Conclusion

We have presented a general methodology for the design of redundant manipulators for dynamic performance. This methodology provides a modular decomposition of the design process into subproblems involving the separate design of the macro and mini manipulators. It was also that adherence to this methodology allows the prediction of bounds on the properties of the overall mechanism. The design process was illustrated on an example of a six DOF planar manipulator. These results can be easily extended to systems involving several macro/mini structures.

Acknowledgments

The financial support of NASA/JPL and Boeing are gratefully acknowledged. Also many thanks to Professor Walter Murray of the Operations Research Department at Stanford University who contributed greatly to the actuator selection algorithm used in this study.

References

[1] Jorge Angeles. The design of isotropic manipulator architectures in the presence of redundancies. *The International Journal of Robotics Research*, 11(3):196–201, June 1992.

[2] Jorge Angeles and Carlos S. Lòpez-Cajùn. Kinematic isotropy and the conditioning index of serial robotic manipulators. *The International Journal of Robotics Research*, 11(6):560–571, December 1992.

[3] Jorge Angeles, F. Ranjbaran, and R. V. Patel. On the design of the kinematic structure of seven-axes redundant manipulators for maximum conditioning. In *Proceedings IEEE International Conference on Robotics and Automation*, volume 1, 1992.

[4] Haruhiko Asada. A geometrical representation of manipulator dynamics and its application to arm design. *Journal of Dynamic Systems, Measurement, and Control*, 105(3):131–135, September 1983.

[5] Alan Bowling. *Analysis of Robotic Manipulator Dynamic Performance: Acceleration and Force Capabilities*. PhD thesis, Stanford University, June 1998.

[6] Alan Bowling and Oussama Khatib. Analysis of the acceleration characteristics of non-redundant manipulators. In *Proceedings IEEE/RSJ International Conference on Intelligent Robots and Systems*, volume 2, pages 323–328. IEEE Computer Society Press, August 1995. Pittsburgh, Pennsylvania.

[7] Alan Bowling and Oussama Khatib. Design of macro/mini manipulators for optimal dynamic performance. In *Proceedings IEEE International Conference on Robotics and Automation*, volume 1, pages 449–454. IEEE Computer Society Press, April 1997. Albuquerque, New Mexico.

[8] Alan Bowling and Oussama Khatib. The motion isotropy hypersurface: A characterization of acceleration capability. In *Proceedings IEEE/RSJ International Conference on Intelligent Robots and Systems*, October 1998. Accepted for Publication.

[9] Subhas Desa and Yong-Yil Kim. The application of acceleration set theory to manipulator design. In *The 21st Biennial Mechanisms Conference: Cams, Gears, Robot and Mechanism Design*, September 1990. Chicago, Illinois.

[10] Clément Gosselin. Dexterity indices for planar and spherical robotic manipulators. In *Proceedings IEEE International Conference on Robotics and Automation*, 1990.

[11] Timothy J. Graettinger and Bruce H. Krogh. The acceleration radius: A global performance measure for robotic manipulators. *IEEE Journal of Robotics and Automation*, 4(1), February 1988.

[12] Thomas R. Kane and David A. Levinson. *Dynamics: Theory and Applications*. McGraw-Hill Book Company, 1985.

[13] Oussama Khatib. Inertial properties in robotic manipulation: An object-level framework. *The International Journal of Robotics Research*, 13(1):19–36, February 1995.

[14] Oussama Khatib and Sunil Agrawal. Isotropic and uniform inertial and acceleration characteristics: Issues in the design of redundant manipulators. In *Proceedings of the IUTAM/IFAC Symposium on Dynamics of Controlled Mechanical Systems*, 1989. Zurich, Switzerland.

[15] Oussama Khatib and Joel Burdick. Optimization of dynamics in manipulator design: The operational space formulation. *The International Journal of Robotics and Automation*, 2(2):90–98, 1987.

[16] Oussama Khatib and Bernard Roth. New robot mechanisms for new robot capabilities. In *Proceedings of the IEEE/RSJ International Conference on Intelligent Robots and Systems*, volume 1, November 1991. Osaka,Japan.

[17] Charles A. Klein and Bruce E. Blaho. Dexterity measures for the design and control of kinematically redundant manipulators. *The International Journal of Robotics Research*, 6(2):72–83, 1987.

[18] Ricardo Matone and Bernard Roth. Designing manipulators for both kinematic and dynamic isotropy. In A. Morecki, G. Bianchi, and C. Rzymkowski, editors, *Proceedings Tenth CISM-IFToMM Symposium on Theory and Practice of Robots and Manipulators (Romansy 11)*, 1997.

[19] R. V. Mayorga, B. Ressa, and A. K. C. Wong. A dexterity measure for robot manipulators. In *Proceedings IEEE International Conference on Robotics and Automation*, volume 1, 1990.

[20] Tsuneo Yoshikawa. Dynamic manipulability of robot manipulators. In *Proceedings 1985 IEEE International Conference on Robotics and Automation*, pages 1033–1038, 1985. St. Louis, Missouri.

[21] Tsuneo Yoshikawa. Manipulability of robotic mechanisms. *The International Journal of Robotics Research*, 4(2), 1985.